NASA Contractor Report 194909

ICASE Report No. 94-30

ICASE

ON THE NONLINEAR STABILITY OF VISCOUS MODES WITHIN THE RAYLEIGH PROBLEM ON AN INFINITE FLAT PLATE

J.C. Webb
S.R. Otto
G.M. Lilley

Contract NAS1-19480
May 1994

Institute for Computer Applications in Science and Engineering
NASA Langley Research Center
Hampton, VA 23681-0001

Operated by Universities Space Research Association

ICASE Fluid Mechanics

Due to increasing research being conducted at ICASE in the field of fluid mechanics, future ICASE reports in this area of research will be printed with a green cover. Applied and numerical mathematics reports will have the familiar blue cover, while computer science reports will have yellow covers. In all other aspects the reports will remain the same; in particular, they will continue to be submitted to the appropriate journals or conferences for formal publication.

ON THE NONLINEAR STABILITY OF VISCOUS MODES WITHIN THE RAYLEIGH PROBLEM ON AN INFINITE FLAT PLATE

J. C. Webb*
Institute for Computer Applications in Science and Engineering
Mail Stop 132c, NASA Langley Research Center
Hampton, VA 23681-0001, USA

S. R. Otto*
School of Maths and Stats
The University of Birmingham
Edgbaston, Birmingham B15 2TT, United Kingdom

G. M. Lilley*
Department of Aeronautics and Astronautics
University of Southampton, United Kingdom

ABSTRACT

The stability has been investigated of the unsteady flow past an infinite flat plate when it is moved impulsively from rest, in its own plane. For small times the instantaneous stability of the flow depends on the linearised equations of motion which reduce in this problem to the Orr-Sommerfeld equation. It is known that the flow for certain values of Reynolds number, frequency and wavenumber is unstable to Tollmien-Schlichting waves, as in the case of the Blasius boundary layer flow past a flat plate. With increase in time, the unstable waves only undergo growth for a finite time interval, and this growth rate is itself a function of time. The influence of finite amplitude effects is studied by solving the full Navier-Stokes equations. It is found that the stability characteristics are markedly changed both by the consideration of the time evolution of the flow, and by the introduction of finite amplitude effects.

* Research was supported by the National Aeronautics and Space Administration under NASA contract No. NAS1–19480 while the authors were in residence at the Institute for Computer Applications in Science and Engineering (ICASE), NASA Langley Research Center, Hampton, VA 23681

§1 Introduction

In the flow over a flat plate at zero pressure gradient the stability of the boundary layer is not only dependent on its instantaneous thickness, but also on its rate of growth. This problem, based on the Blasius mean flow has been studied extensively. However, experiment shows that the stability characteristics based on the local growth of the boundary layer provide a good approximate model. This was confirmed in the triple-deck structure calculations of Smith (1979a) on the influence of the rate of growth of near neutral unstable Tollmien-Schlichting (TS) modes at high Reynolds numbers. The weakly nonlinear evolution of TS modes within a Blasius layer was studied by Smith (1979b) and Hall & Smith (1984). In the latter of these studies, it was demonstrated how a linear mode could evolve smoothly into a finite amplitude perturbation. In Otto (1994), this was shown to be feasible within the unsteady problem. Smith also found that it was not possible to determine the effects of boundary layer spatial growth on the stability of the modes since different conclusions were found depending on which flow quantity was used to express the finite amplitude of a mode. Gaster (1974) and Eagles & Weissman (1975) have also contributed to our understanding of the Blasius problem. In this flow, Tollmien-Schlichting waves grow spatially in the flow direction and the resulting equations in this coordinate are elliptic, and are computationally expensive to solve. The approach of Bertolotti (1991), using the Parabolised Stability Equations (PSE), in which the elliptic equations are made parabolic on the assumption of slowly evolving wave characteristics and the changes in structure may be locally assumed linear, has been one of the more successful methods to reduce the computational cost. This approach allows far larger steps to be taken in the evolutionary coordinate.

In the present work, the related temporal problem is considered. Otto (1994) found reasonable agreement between triple-deck and Orr-Sommerfeld results in regimes of common validity, for the unsteady flow problem of the flat plate moved impulsively from rest. Here, we discuss both the linear and nonlinear problems, and since our

problem is already parabolic in the evolutionary coordinate, we use the PSE methodology to study the effects of finite amplitude and to reduce the number of time steps per period required for accuracy, which it does very effectively. We find substantial differences between the results of linear theory based on the Orr-Sommerfeld equations and our results for finite amplitude waves.

In Section 2, we derive equations for the linear and nonlinear evolution of Tollmien-Schlichting waves with a brief summary of our period fitting technique. Section 3 contains details of the numerical methods used to solve the equations. In Section 4, we discuss the results and finally in Section 5, we draw some conclusions.

§2 Formulation

The physical problem consists of an infinite flat plate in two dimensions which is at rest within a fluid of density ρ_0 and pressure p_0. At time $t = 0$, the plate is moved impulsively from rest with the speed U_0, in the direction parallel to its alignment (see Figure 2.1).

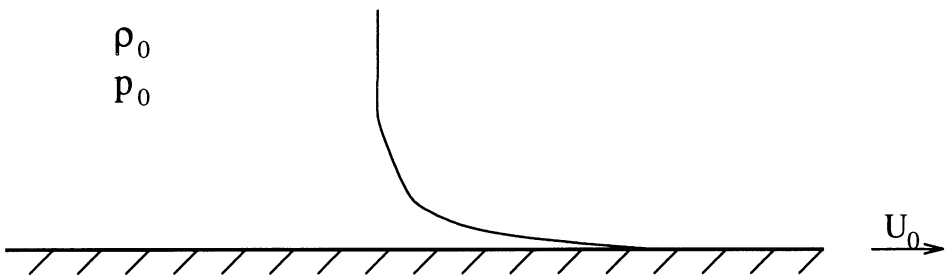

Figure 2.1 Velocity Profile Due to Impulsive Motion of Flat Plate

The governing equations for this problem are the equation of continuity and the Navier-Stokes equations

$$\begin{aligned} \frac{\partial u}{\partial x} + \frac{\partial v}{\partial y} &= 0 \\ \frac{\partial u}{\partial t} + u\frac{\partial u}{\partial x} + v\frac{\partial u}{\partial y} &= -\frac{\partial p}{\partial x} + \frac{1}{Re}\nabla^2 u \\ \frac{\partial v}{\partial t} + u\frac{\partial v}{\partial x} + v\frac{\partial v}{\partial y} &= -\frac{\partial p}{\partial y} + \frac{1}{Re}\nabla^2 v \end{aligned} \tag{2.1}$$

where each variable is dimensionless, with scaling parameters ρ_0, U_0, μ_0, and L representing the ambient density, plate velocity, viscosity and a unit of length in the flow direction, respectively. The Reynolds number per unit length of plate, Re is defined as

$$Re = \frac{LU_0\rho_0}{\mu_0} \tag{2.2}$$

and ∇^2 is the two-dimensional Laplacian operator

$$\nabla^2 = \frac{\partial^2}{\partial x^2} + \frac{\partial^2}{\partial y^2}. \tag{2.3}$$

We note that the pressure has been non-dimensionalised by $\rho_0 U_0^2$ and time by $\frac{U_0}{L}$.

In the case of an infinite plate impulsively set in motion, the *mean* solution, *i.e.* the undisturbed flow, is given in dimensionless terms by the reduced set of equations

$$\begin{aligned} \frac{\partial \bar{u}}{\partial t} &= \frac{1}{Re}\frac{\partial^2 \bar{u}}{\partial y^2} \\ \bar{v} &= 0 \\ \bar{p} &= \frac{p_0}{\rho_0 U_0^2} \end{aligned} \tag{2.4}$$

with initial and boundary conditions

$$\begin{aligned} \bar{u}(0,t) &= \begin{cases} 0 & t = 0 \\ 1 & t > 0 \end{cases} \\ \bar{u}(Y,t) &\to 0 \qquad Y \to \infty \end{aligned} \tag{2.5}$$

The mean streamwise velocity component is therefore given exactly by

$$\bar{u}(y,t) = 1 - \mathrm{erf}\left(\frac{y\sqrt{Re}}{2\sqrt{t}}\right). \tag{2.6}$$

Given the form of (2.6), it is appropriate to choose physical variables X and Y that absorb the $\sqrt{Re}$ dependence,

$$\begin{aligned} X &= x\sqrt{Re} \\ Y &= y\sqrt{Re} \end{aligned} . \tag{2.7}$$

With this transformation, the governing set of equations become

$$\begin{aligned} \frac{\partial u}{\partial X} + \frac{\partial v}{\partial Y} &= 0 \\ \frac{1}{\sqrt{Re}}\frac{\partial u}{\partial t} + u\frac{\partial u}{\partial X} + v\frac{\partial u}{\partial Y} &= -\frac{\partial p}{\partial X} + \frac{1}{\sqrt{Re}}\nabla^2 u \\ \frac{1}{\sqrt{Re}}\frac{\partial v}{\partial t} + u\frac{\partial v}{\partial X} + v\frac{\partial v}{\partial Y} &= -\frac{\partial p}{\partial Y} + \frac{1}{\sqrt{Re}}\nabla^2 v \end{aligned} \tag{2.8}$$

and the mean flow is now given by

$$\bar{u}(Y,t) = 1 - \mathrm{erf}\left(\frac{Y}{2\sqrt{t}}\right). \tag{2.9}$$

The lack of a physical boundary condition for pressure provides a computational difficulty for equations (2.8) cast in terms of the primitive variables. We avoid this problem by reducing this set of equations to a single equation for the normal velocity

component. In this section, we will discuss the analysis for both linear and nonlinear disturbances. In addition, we show how to generate an appropriate initial condition to begin the stability calculation, and introduce a period-fitting technique intended to reduce the total computational effort.

2.1 Linear Disturbance Equations

We let $\tilde{u}$, $\tilde{v}$ and $\tilde{p}$ represent disturbances from the mean state:

$$\begin{aligned} u(X,Y,t) &= \bar{u}(Y,t) + \tilde{u}(X,Y,t)\,, \\ v(X,Y,t) &= \tilde{v}(X,Y,t)\,, \\ p(X,Y,t) &= \frac{p_0}{\rho_0 U_0^2} + \tilde{p}(X,Y,t)\,. \end{aligned} \tag{2.10}$$

After substituting equations (2.10) into equations (2.8) and linearizing the resulting expressions, the perturbation pressure, $\tilde{p}$, and the streamwise velocity component, $\tilde{u}$, may be eliminated, giving the following single equation for $\tilde{v}$, the transverse component:

$$\left[\Big(\frac{1}{\sqrt{Re}}\frac{\partial}{\partial t} + \bar{u}\frac{\partial}{\partial X} - \frac{1}{\sqrt{Re}}\big(\frac{\partial^2}{\partial X^2} + \frac{\partial^2}{\partial Y^2}\big)\Big)\big(\frac{\partial^2}{\partial X^2} + \frac{\partial^2}{\partial Y^2}\big) - \frac{\partial^2 \bar{u}}{\partial Y^2}\frac{\partial}{\partial X}\right]\tilde{v} = 0. \tag{2.11}$$

The physical problem is spatially homogeneous in the X-direction, and it is legitimate to assume a periodic X-variation, giving

$$\tilde{v}(X,Y,t) = \hat{v}(Y,t)\,\mathrm{e}^{i\alpha X} \tag{2.12}$$

which reduces (2.11) to

$$\left[\big(\frac{i}{\sqrt{Re}}\frac{\partial}{\partial t} - \alpha\bar{u}\big)\big(\frac{\partial^2}{\partial Y^2} - \alpha^2\big) + \alpha\frac{\partial^2 \bar{u}}{\partial Y^2} + \frac{1}{i\sqrt{Re}}\big(\frac{\partial^4}{\partial Y^4} - 2\alpha^2\frac{\partial^2}{\partial Y^2} + \alpha^4\big)\right]\hat{v} = 0. \tag{2.13}$$

When a periodic time dependence, $\mathrm{e}^{-i\omega t}$, is assumed, and noting the mean velocity is a function of Y and t only, equation (2.13) reduces to the familiar Orr-Sommerfeld equation with similar results. In our case, we consider the solution to equation (2.13) at any fixed time and then the results show the local stability characteristics of the

flow for the linear problem. For this time-dependent problem, the boundary conditions are

$$\hat{v}(0,t) = 0, \tag{2.14}$$

and since $\frac{\partial \tilde{u}}{\partial X} = 0$ at $Y = 0$,

$$\frac{\partial \hat{v}}{\partial Y}(0,t) = 0. \tag{2.15}$$

In the farfield, as $Y \to \infty$, the solution depends on $\mathrm{e}^{-\alpha Y}$, giving for large Y,

$$\begin{array}{ll} \frac{\partial \hat{v}(Y,t)}{\partial Y} + \alpha \hat{v}(Y,t) = 0 & \\ \frac{\partial^2 \hat{v}(Y,t)}{\partial^2 Y} - \alpha^2 \hat{v}(Y,t) = 0 & \end{array} \qquad Y \to \infty\,. \tag{2.16}$$

2.2 Nonlinear Disturbance Equations

Substituting (2.10) into (2.8), retaining the nonlinear terms, and eliminating the perturbation pressure, we find the following for $\tilde{v}$:

$$\begin{aligned} &\left[\Big(\frac{1}{\sqrt{Re}}\frac{\partial}{\partial t} + \bar{u}\frac{\partial}{\partial X} - \frac{1}{\sqrt{Re}}\big(\frac{\partial^2}{\partial X^2} + \frac{\partial^2}{\partial Y^2}\big)\Big)\big(\frac{\partial^2}{\partial X^2} + \frac{\partial^2}{\partial Y^2}\big) - \frac{\partial^2 \bar{u}}{\partial Y^2}\frac{\partial}{\partial X}\right]\tilde{v} = \\ &-\Big(\tilde{u}\frac{\partial}{\partial X} + \tilde{v}\frac{\partial}{\partial Y}\Big)\Big(\frac{\partial^2}{\partial X^2} + \frac{\partial^2}{\partial Y^2}\Big)\tilde{v} + \frac{\partial \tilde{v}}{\partial Y}\Big(\frac{\partial^2}{\partial X^2} + \frac{\partial^2}{\partial Y^2}\Big)\tilde{v} + \frac{\partial \tilde{v}}{\partial X}\Big(\frac{\partial^2}{\partial X^2} + \frac{\partial^2}{\partial Y^2}\Big)\tilde{u}\,. \end{aligned} \tag{2.17}$$

The $\frac{\partial^2 \tilde{u}}{\partial X^2}$ could be eliminated using the continuity equation. However, since the $\frac{\partial^2 \tilde{u}}{\partial Y^2}$ term cannot, we leave both terms in for ease of presentation.

We now express the disturbance quantities as a finite sum of modes with respect to the wavenumber alpha:

$$\begin{aligned} \tilde{v}(X,Y,t) &= \sum_{j=-M}^{M} \hat{v}_j(Y,t)\mathrm{e}^{ij\alpha X}, \\ \tilde{u}(X,Y,t) &= \sum_{j=-M}^{M} \hat{u}_j(Y,t)\mathrm{e}^{ij\alpha X}, \\ \tilde{p}(X,Y,t) &= \sum_{j=-M}^{M} \hat{p}_j(Y,t)\mathrm{e}^{ij\alpha X}. \end{aligned} \tag{2.18}$$

The continuity equation allows for elimination of all the $\hat{u}_j$'s, except $\hat{u}_0$, in favour of the $\hat{v}_j$'s and requires that $\hat{v}_0(Y,t) = 0$. The resulting equation after making these

substitutions in (2.17) and neglecting all products which combine to give a mode beyond M is given by

$$\left[\left(\frac{i}{\sqrt{Re}}\frac{\partial}{\partial t} - j\alpha\bar{u} + \frac{1}{i\sqrt{Re}}\left(\frac{\partial^2}{\partial Y^2} - j^2\alpha^2\right)\right)\left(\frac{\partial^2}{\partial Y^2} - j^2\alpha^2\right) + j\alpha\frac{\partial^2\bar{u}}{\partial Y^2}\right]\hat{v}_j = \mathrm{N}\hat{v} \quad (2.19)$$

where

$$\begin{aligned}\mathrm{N}\hat{v} = i\sum_{\substack{k=-M\\k\neq 0,j}}^{M+j}&\left[jk\alpha^2\left(\frac{\partial\hat{v}_k}{\partial Y}\hat{v}_{j-k} - \frac{k}{j-k}\hat{v}_k\frac{\partial\hat{v}_{j-k}}{\partial Y}\right) + \frac{j}{j-k}\frac{\partial^2\hat{v}_k}{\partial Y^2}\frac{\partial\hat{v}_{j-k}}{\partial Y} - \frac{j}{k}\frac{\partial^3\hat{v}_k}{\partial Y^3}\hat{v}_{j-k}\right]\\ &+ j\alpha\left(\hat{u}_0\frac{\partial^2\hat{v}_j}{\partial Y^2} - j^2\alpha^2\hat{u}_0\hat{v}_j - \frac{\partial^2\hat{u}_0}{\partial Y^2}\hat{v}_j\right)\end{aligned} \quad (2.20)$$

for $j = -M, -M+1, -M+2, ..., -1$, and

$$\begin{aligned}\mathrm{N}\hat{v} = i\sum_{\substack{k=-M+j\\k\neq 0,j}}^{M}&\left[jk\alpha^2\left(\frac{\partial\hat{v}_k}{\partial Y}\hat{v}_{j-k} - \frac{k}{j-k}\hat{v}_k\frac{\partial\hat{v}_{j-k}}{\partial Y}\right) + \frac{j}{j-k}\frac{\partial^2\hat{v}_k}{\partial Y^2}\frac{\partial\hat{v}_{j-k}}{\partial Y} - \frac{j}{k}\frac{\partial^3\hat{v}_k}{\partial Y^3}\hat{v}_{j-k}\right]\\ &+ j\alpha\left(\hat{u}_0\frac{\partial^2\hat{v}_j}{\partial Y^2} - j^2\alpha^2\hat{u}_0\hat{v}_j - \frac{\partial^2\hat{u}_0}{\partial Y^2}\hat{v}_j\right)\end{aligned} \quad (2.21)$$

for $j = 1, 2, 3, ..., M$.

The boundary conditions for the $\hat{v}_j$'s are analagous to those for the linear case:

$$\begin{aligned}&\hat{v}_j(0,t) = 0, \quad \tfrac{\partial\hat{v}_j}{\partial Y}(0,t) = 0,\\ &\tfrac{\partial\hat{v}_j(Y,t)}{\partial Y} + j\alpha\hat{v}_j(Y,t) = 0 \qquad Y\to\infty.\\ &\tfrac{\partial^2\hat{v}_j(Y,t)}{\partial^2 Y} - j^2\alpha^2\hat{v}_j(Y,t) = 0\end{aligned} \quad (2.22)$$

The variable $\hat{u}_0(Y,t)$ has no associated wavy part, and is effectively a correction to the mean solution due to the presence of the finite amplitude waves. An equation for it may be found by looking at the non-wavy component of the x-momentum equation, after substituting in (2.18):

$$\frac{\partial\hat{u}_0}{\partial t} - \frac{\partial^2\hat{u}_0}{\partial Y^2} = -\sqrt{Re}\sum_{\substack{k=-M\\k\neq 0}}^{M}\frac{i}{k\alpha}\frac{\partial^2\hat{v}_k}{\partial Y^2}\hat{v}_{-k}. \quad (2.23)$$

The boundary conditions for $\hat{u}_0$ consist of a no-slip condition at the wall and an asymptotic condition far away from the wall:

$$\hat{u}_0(0,t) = 0, \qquad \frac{\partial \hat{u}_0(Y,t)}{\partial Y} = 0 \quad Y \to \infty\,. \tag{2.24}$$

The system of equations (2.19) through (2.24) define the nonlinear problem.

2.3 Initial Condition

In order to solve either the linear or nonlinear problem for some time $t = t_0 > 0$, we need to define an initial perturbation which is at least an approximate solution of the linearised equations. To this end, we can freeze the flow at a given time and determine the local stability characteristics of the flow from an Orr-Sommerfeld (OS) analysis. In particular, for given values of α and $\sqrt{Re}$, we can determine a function $\check{v}(Y)$ and a frequency ω, such that an initial disturbance of the form $\check{v}(Y)\mathrm{e}^{i\alpha X}$ will behave according to $\check{v}(Y)\mathrm{e}^{i\alpha X - i\omega t}$ for all time for the frozen flow.

However, since the OS equation does not allow for the evolution of the undisturbed flow with time, using an initial condition constructed in this way generates spurious oscillations in the solution. We overcome this problem by finding an initial condition, which is a slight perturbation of the OS eigenfunction $\check{v}(Y)$, that is sensitive to the changing *mean* flow. Following the approach of Bertolotti, we let

$$\hat{v}(Y,t) = v'(Y,t)\mathrm{e}^{-i\int_0^t \theta(\eta)d\eta} \tag{2.25}$$

where it is assumed that the time dependence of v' is slowly varying. Substituting this expression into the linear stability equation (2.13) gives

$$\begin{aligned}\left(\tfrac{\theta(t)}{\sqrt{Re}} - \alpha\bar{u}(Y,t)\right)\left(\frac{\partial^2}{\partial Y^2} - \alpha^2\right)v'(Y,t) + \alpha\tfrac{\partial^2\bar{u}}{\partial Y^2}v'(Y,t)\\ + \tfrac{1}{i\sqrt{Re}}\left(\tfrac{\partial^4}{\partial Y^4} - 2\alpha^2\tfrac{\partial^2}{\partial Y^2} + \alpha^4\right)v'(Y,t) = -\tfrac{i}{\sqrt{Re}}\left(\tfrac{\partial^2}{\partial Y^2} - \alpha^2\right)\tfrac{\partial v'(Y,t)}{\partial t}\,.\end{aligned} \tag{2.26}$$

We now make a 1st order Taylor Series approximation about t_0:

$$
\begin{aligned}
&t \approx t_0 + \tau\,, \\
&\theta \approx \theta(t_0) + \tau \tfrac{\partial \theta}{\partial t}(t_0) = \theta_0 + \tau\theta_1\,, \\
&v'(Y,t) \approx v'(Y,t_0) + \tau \tfrac{\partial v'}{\partial t}(Y,t_0) = v_0'(Y) + \tau v_1'(Y)\,, \\
&\tfrac{\partial v'(Y,t)}{\partial t} \approx \tfrac{\partial v'}{\partial t}(Y,t_0) = v_1'(Y)\,, \\
&\bar{u}(Y,t) \approx \bar{u}(Y,t_0) + \tau \tfrac{\partial \bar{u}}{\partial t}(Y,t_0)\,, \\
&\tfrac{\partial^2 \bar{u}(Y,t)}{\partial Y^2} \approx \tfrac{\partial^2 \bar{u}}{\partial Y^2}(Y,t_0) + \tau \tfrac{\partial^3 \bar{u}}{\partial t \partial Y^2}(Y,t_0)\,.
\end{aligned}
\tag{2.27}
$$

We note that the approximation for $\frac{\partial v'(Y,t)}{\partial t}$ does not include a $\frac{\partial^2 v'}{\partial t^2}(Y,t_0)$ term; the slow variation of v' with t allows us to ignore the second derivative. Collecting like powers of τ, namely τ^0 and τ^1, we have the following equations, respectively:

$$
\begin{aligned}
\mathrm{L}v_0'(Y) &= -i\Big(\tfrac{\partial^2}{\partial Y^2} - \alpha^2\Big)v_1'(Y) \\
\mathrm{L}v_1'(Y) &= -\Big(\tfrac{\theta_1}{\sqrt{Re}} - \alpha \tfrac{\partial \bar{u}}{\partial t}(Y,t_0)\Big)\Big(\tfrac{\partial^2}{\partial Y^2} - \alpha^2\Big)v_0'(Y) - \alpha \tfrac{\partial^3 \bar{u}}{\partial t \partial Y^2}(Y,t_0)v_0'(Y)
\end{aligned}
\tag{2.28}
$$

where L is the Orr-Sommerfeld operator

$$
\mathrm{L} = \Big(\tfrac{\theta_0}{\sqrt{Re}} - \alpha\bar{u}(Y,t_0)\Big)\Big(\tfrac{\partial^2}{\partial Y^2} - \alpha^2\Big) + \alpha \tfrac{\partial^2 \bar{u}}{\partial Y^2}(Y,t_0) + \tfrac{i}{\sqrt{Re}}\Big(\tfrac{\partial^4}{\partial Y^4} - 2\alpha^2 \tfrac{\partial^2}{\partial Y^2} + \alpha^4\Big). \tag{2.29}
$$

The boundary conditions for v_0' and v_1' are given by (2.14), (2.15), and (2.16).

With the additional constraint that v_0' and v_1' are orthogonal,

$$
\int_0^\infty (v_0')^* v_1' \,\mathrm{d}Y = 0, \tag{2.30}
$$

equations (2.28) provide an eigenvalue problem which, when solved, gives an initial profile $v_0'(Y)$ and frequency θ_0 which, to first order, take into account the evolution of the undisturbed flow.

To further improve the quality of the initial condition, a higher order version of the above can be performed. In this case, we use a second order Taylor Series approximation, and include the second derivative of v' with respect to t, but ignore the third derivative. In addition to θ_0, θ_1, v_0' and v_1', the resulting eigenvalue problem contains unknowns θ_2 and v_2' which represent the second-order Taylor Series terms. Extending

the above analysis to 2nd order gives a linear equation for v_2' and an orthogonality condition, analagous to (2.30).

2.4 Period Fitting

As mentioned in the previous section, we can separate $\hat{v}(Y,t)$, for the linear case, into a time periodic part, and a function $v'(Y,t)$ that varies slowly with time. In this case, we will write $\hat{v}$ as

$$\hat{v}(Y,t) = v'(Y,t)\mathrm{e}^{-i\omega t} \tag{2.31}$$

where ω is taken to be a real quantity; the growth or decay is represented by the t-variation of v'. To adequately resolve the oscillatory part requires many time steps per period of oscillation. However, the temporal resolution requirements of v' are far less restrictive. Consequently, it is more efficient to remove the periodic part of the solution from the equations and compute only the slowly varying function v'. Substituting (2.31) into the linear disturbance equation (2.13), we find the following equation for v'

$$\begin{aligned}\tfrac{i}{\sqrt{Re}}\left(\tfrac{\partial^2}{\partial Y^2}-\alpha^2\right)\tfrac{\partial v'(Y,t)}{\partial t} + \left(\tfrac{\omega}{\sqrt{Re}}-\alpha\bar{u}(Y,t)\right)\left(\tfrac{\partial^2}{\partial Y^2}-\alpha^2\right)v'(Y,t) + \alpha\tfrac{\partial^2\bar{u}(Y,t)}{\partial Y^2}v'(Y,t)\\ + \tfrac{1}{i\sqrt{Re}}\left(\tfrac{\partial^4}{\partial Y^4}-2\alpha^2\tfrac{\partial^2}{\partial Y^2}+\alpha^4\right)v'(Y,t) = 0\,.\end{aligned} \tag{2.32}$$

Since the extent of the flow increases as $\sqrt{t}$, the value of ω changes with time. Therefore, to implement (2.32), we must be able to estimate ω at any given time. We define the energy $E(Y,t)$ in the following way:

$$E(Y,t) = \int_0^\infty \hat{v}^2(Y,t)\mathrm{d}Y = \int_0^\infty v'^2(Y,t)\mathrm{e}^{-2i\omega t}\mathrm{d}Y\,. \tag{2.33}$$

Ignoring the slow changes of v' and ω with time, we approximate ω by $-\frac{1}{2iE}\frac{\partial E}{\partial t}$.

However, we wish now to work only with v'. Initially, we use a value of ω in (2.32) given by the OS analysis or by the method described in Section 2.3 above. At each time step, we can correct this value by recognizing that the computed value of v'

will contain the slowly changing envelope plus an oscillatory part with a very small frequency that represents the change in ω, *i.e.*

$$\begin{aligned} E'(Y,t) &= \int_0^\infty \hat{v}'^2(Y,t)\mathrm{d}Y, \\ \Delta\omega &\approx -\tfrac{1}{2iE'}\tfrac{\partial E'}{\partial t}, \\ \omega_{\text{new}} &= \omega_{\text{old}} + \Delta\omega. \end{aligned} \tag{2.34}$$

For the nonlinear case, the procedure is very similar. Given that we have

$$\alpha_j = j\alpha \tag{2.35}$$

we make the assumption

$$\omega_j = j\omega. \tag{2.36}$$

That is, we compute ω_1, associated with the fundamental mode, by the method shown in equation (2.34). Then all ω_j for higher order modes are given by (2.36). We note that any errors incurred by this approximation are at least partially corrected by the the time dependence of v'_j.

The nonlinear disturbance equations for the $v'_j s$ now become

$$\begin{aligned} \tfrac{i}{\sqrt{Re}}\left(\tfrac{\partial^2}{\partial Y^2} - j^2\alpha^2\right)\tfrac{\partial v'_j(Y,t)}{\partial t} + j\left(\tfrac{\omega}{\sqrt{Re}} - \alpha\bar{u}(Y,t)\right)\left(\tfrac{\partial^2}{\partial Y^2} - j^2\alpha^2\right)v'_j(Y,t) + j\alpha\tfrac{\partial^2\bar{u}(Y,t)}{\partial Y^2}v'_j(Y,t) \\ + \tfrac{1}{i\sqrt{Re}}\left(\tfrac{\partial^4}{\partial Y^4} - 2j^2\alpha^2\tfrac{\partial^2}{\partial Y^2} + j^4\alpha^4\right)v'_j(Y,t) = \mathrm{N}v' \end{aligned} \tag{2.37}$$

where $\mathrm{N}v'$ has the same form as given in (2.20) except that $\hat{v}$ is replaced everywhere by v'.

§3 Numerical Methods

In this section, we will provide some of the pertinent details of the numerical solution of both the linear and nonlinear problems. We begin with a brief discussion of the grid and spectral discretization, and follow with descriptions of the initial condition generation, linear simulations and nonlinear simulations.

3.1 Discretization

The mean solution is given by equation (2.9) which is repeated here:

$$\bar{u}(Y,t) = 1 - \mathrm{erf}\left(\frac{Y}{2\sqrt{t}}\right). \tag{3.1}$$

Although, u is technically finite for any finite Y and t, it decays quickly away from the plate, and from a computational standpoint, it is appropriate to define the extent of the undisturbed flow to be the Y value at which the undisturbed velocity is 1% of the plate speed. Since typically the OS eigensolutions decay slowly relative to the decay of the undisturbed flow solution, it is necessary to choose a physical domain that extends well beyond this limit. Defining the edge of the undisturbed flow at $t = t_0$ to be

$$Y_{\mathrm{ed}} \ni \frac{u(Y_{\mathrm{ed}}, t_0)}{U_0} = 1 - \mathrm{erf}\left(\frac{Y_{\mathrm{ed}}}{2\sqrt{t_0}}\right) = 0.01, \tag{3.2}$$

we have $Y_{\mathrm{ed}} = 1.821(2\sqrt{t_0})$. We choose an upper bound for Y to be

$$Y_{\mathrm{max}} = 40\sqrt{t_0}, \tag{3.3}$$

i.e. our domain extends to about 10 times the initial undisturbed flow extent.

We employ a Chebyshev collocation discretization using $N = 80$ polynomials. Although the disturbances do not require any local resolution because, once introduced, they extend throughout the domain, the mean solution decays rapidly away from the wall. Consequently, we use a mapping which maps 0 to Y_{max} onto [-1,1] as required by the spectral discretization, but does so in such a way that points are concentrated near the lower boundary. The computational coordinate η is defined as follows:

$$\eta = \frac{bY - c}{Y + c} \tag{3.4}$$

where b and c are chosen so that $Y(1) = Y_{\max}$ and $Y(0) = Y_{\text{mid}}$ The value of Y_{mid} is the physical coordinate that bisects the grid. We take it to be $15\sqrt{t_0}$, or about 4 times the initial undisturbed flow extent. This allows for the undisturbed flow to grow in extent during the simulation, and keeps the stretching from being too severe. With these stipulations we have

$$\begin{aligned} c &= \frac{Y_{\max} Y_{\text{mid}}}{Y_{\max} - 2Y_{\text{mid}}} \\ b &= 1 + 2\frac{c}{Y_{\max}} \end{aligned} \quad . \tag{3.5}$$

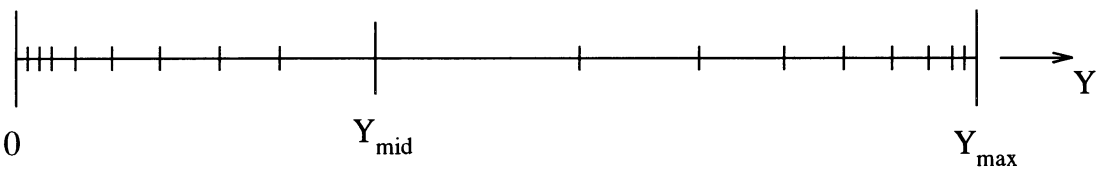

Figure 3.1 Representation of Stretched Spectral Grid

3.2 Initial Conditions

For both the linear and nonlinear simulations, the disturbances are introduced at dimensionless time $t_0 = 0.25$. We generate three sets of initial conditions at this t_0. The first corresponds to the OS eigenfunction, and the remaining two are the 1st and 2nd order corrections, respectively, of §2.3.

The continuous Orr-Sommerfeld eigenvalue problem is defined by

$$\mathrm{L}v_0'(Y) \doteq 0 \tag{3.6}$$

and the boundary conditions

$$\begin{aligned} & v_0'(0) = 0, \quad \frac{\partial v_0'}{\partial Y}(0) = 0, \\ & \frac{\partial v_0'(Y)}{\partial Y} + \alpha v_0'(Y) = 0 \\ & \frac{\partial^2 v_0'(Y)}{\partial Y^2} - \alpha^2 v_0'(Y) = 0 \qquad Y \to \infty, \end{aligned} \tag{3.7}$$

where L is the Orr-Sommerfeld operator given by equation (2.29). The corresponding discrete problem replaces $\frac{\partial}{\partial Y}$ with the discrete operator $\left(\frac{\mathrm{D}}{\mathrm{D}Y}\right)_l$, where given a discrete function ϕ defined on the nodes $l = 0, 1, 2, ..., N$,

$$\left(\frac{\mathrm{D}\phi}{\mathrm{D}Y}\right)_l = \left(\frac{\partial \eta}{\partial Y}\right)_l \sum_{k=0}^{N} d_{l,k}\phi_k, \tag{3.8}$$

where, once again, $\eta \in [-1,1]$ is the computational coordinate. The $d_{l,k}$'s are the coefficients of the Chebyshev 1st derivative matrix. The system is then defined by applying the discrete OS equation at the interior nodes $2,3,4,...,N-2$, and the discrete wall and asymptotic boundary conditions at $\eta = -1$ $(Y = 0)$ and $\eta = 1$ $(Y = Y_{\max})$ respectively.

For a given α and $\sqrt{Re}$, the solution of this eigenvalue problem provides a frequency ω and an initial profile $v_l^0, l = 0,1,2,...,N$, which may be used to start the linear simulation.

In the nonlinear case, this profile may be used as the starting value for the fundamental mode. In these simulations, we set the higher order modes initially to 0, and the -1 mode to the complex conjugate of the fundamental.

The discrete analogues to the 1st and 2nd order correction problems of §2.3 follow directly from above. The resulting linear systems are also eigenvalue problems, the solutions of which provide a frequency and initial profile.

3.3 Linear Simulations

The continuous linear problem is defined by equation (2.13) with boundary conditions (2.14), (2.15), and (2.16) and initial condition provided as in the the above section. We employ the discrete form of these equations along with the Crank-Nicolson time differencing, given by

$$\frac{\hat{v}_l^{n+1}-\hat{v}_l^n}{\Delta t} = \frac{1}{2}\left(\frac{\partial \hat{v}_l^{n+1}}{\partial t} + \frac{\partial \hat{v}_l^n}{\partial t}\right), \tag{3.9}$$

which results in the following linear set of equations for $\hat{v}_l^{n+1}$:

$$\begin{aligned}
&\Bigg[\left(\frac{i}{\sqrt{Re}} - \frac{1}{2}\alpha\bar{u}_l^{n+1}\Delta t\right)\left(\left(\frac{\mathrm{D}}{\mathrm{DY}}\right)^2 - \alpha^2\right) + \frac{1}{2}\alpha\left(\frac{\partial^2\bar{u}}{\partial Y^2}\right)_l^{n+1}\Delta t \\
&\qquad + \frac{\Delta t}{2i\sqrt{Re}}\left(\left(\frac{\mathrm{D}}{\mathrm{DY}}\right)^4 - 2\alpha^2\left(\frac{\mathrm{D}}{\mathrm{DY}}\right)^2 + \alpha^4\right)\Bigg]\hat{v}_l^{n+1} \\
&= \Bigg[\left(\frac{i}{\sqrt{Re}} + \frac{1}{2}\alpha\bar{u}_l^{n}\Delta t\right)\left(\left(\frac{\mathrm{D}}{\mathrm{DY}}\right)^2 - \alpha^2\right) - \frac{1}{2}\alpha\left(\frac{\partial^2\bar{u}}{\partial Y^2}\right)_l^{n}\Delta t \\
&\qquad - \frac{\Delta t}{2i\sqrt{Re}}\left(\left(\frac{\mathrm{D}}{\mathrm{DY}}\right)^4 - 2\alpha^2\left(\frac{\mathrm{D}}{\mathrm{DY}}\right)^2 + \alpha^4\right)\Bigg]\hat{v}_l^{n} \qquad l = 2,3,4,...,N-2\,,
\end{aligned} \tag{3.10}$$

and

$$\begin{aligned}
\hat{v}_0^{n+1} &= 0, & \left(\frac{\mathrm{D}\hat{v}^{n+1}}{\mathrm{DY}}\right)_0 &= 0, \\
\left(\frac{\mathrm{D}}{\mathrm{DY}} + \alpha\right)\hat{v}_N^{n+1} &= 0, & \left(\left(\frac{\mathrm{D}}{\mathrm{DY}}\right)^2 - \alpha^2\right)\hat{v}_N^{n+1} &= 0\,.
\end{aligned}$$

The value of N for all simulations is chosen to be $N = 80$.

To perform the simulation with period fitting, we implement the discrete form of (2.32) along with the Crank-Nicolson time differencing (3.9) and the appropriate boundary conditions. This linear set of equations for $(v')_l^{n+1}$, $l = 0, 1, 2, ..., N$ is given by

$$\begin{aligned}
&\Bigg[\Big(\tfrac{i}{\sqrt{Re}} + \tfrac{\Delta t}{2}\big(\tfrac{\omega}{\sqrt{Re}} - \alpha\bar{u}_l^{n+1}\big)\Big)\Big(\big(\tfrac{\mathrm{D}}{\mathrm{DY}}\big)^2 - \alpha^2\Big) + \tfrac{1}{2}\alpha\big(\tfrac{\partial^2\bar{u}}{\partial Y^2}\big)_l^{n+1}\Delta t \\
&\qquad + \tfrac{\Delta t}{2i\sqrt{Re}}\Big(\big(\tfrac{\mathrm{D}}{\mathrm{DY}}\big)^4 - 2\alpha^2\big(\tfrac{\mathrm{D}}{\mathrm{DY}}\big)^2 + \alpha^4\Big)\Bigg](v')_l^{n+1} \\
&= \Bigg[\Big(\tfrac{i}{\sqrt{Re}} - \tfrac{\Delta t}{2}\big(\tfrac{\omega}{\sqrt{Re}} - \alpha\bar{u}_l^{n}\big)\Big)\Big(\big(\tfrac{\mathrm{D}}{\mathrm{DY}}\big)^2 - \alpha^2\Big) - \tfrac{1}{2}\alpha\big(\tfrac{\partial^2\bar{u}}{\partial Y^2}\big)_l^{n}\Delta t \\
&\qquad - \tfrac{\Delta t}{2i\sqrt{Re}}\Big(\big(\tfrac{\mathrm{D}}{\mathrm{DY}}\big)^4 - 2\alpha^2\big(\tfrac{\mathrm{D}}{\mathrm{DY}}\big)^2 + \alpha^4\Big)\Bigg](v')_l^{n} \qquad l = 2, 3, 4, ..., N-2\,,
\end{aligned} \tag{3.11}$$

and

$$(v')_0^{n+1} = 0, \qquad \tfrac{\mathrm{D}}{\mathrm{DY}}(v')_0^{n+1} = 0,$$
$$\Big(\tfrac{\mathrm{D}}{\mathrm{DY}} + \alpha\Big)(v')_N^{n+1} = 0, \quad \Big(\big(\tfrac{\mathrm{D}}{\mathrm{DY}}\big)^2 - \alpha^2\Big)(v')_N^{n+1} = 0\,.$$

3.4 Nonlinear Simulations

The continuous equations for the nonlinear case are given by equations (2.19) through (2.24). The time differencing will once again be of the form (3.9). The resulting discrete set of equations is nonlinear, requiring iterative solution. Consequently, we will verify results by also performing a simulation which uses Crank-Nicolson for the linear left-hand side of equation (2.19) and explicit 2nd order Adams-Bashforth for the nonlinear terms on the right-hand side.

For the explicit treatment of the nonlinear terms, we have the following discrete

analogue to equations (2.19) through (2.21):

$$
\begin{aligned}
&\Bigg[\Big(\tfrac{i}{\sqrt{Re}} - \tfrac{1}{2}j\alpha\bar{u}_l^{n+1}\Delta t\Big)\Big(\big(\tfrac{\mathrm{D}}{\mathrm{DY}}\big)^2 - j^2\alpha^2\Big) + \tfrac{1}{2}j\alpha\big(\tfrac{\partial^2\bar{u}}{\partial Y^2}\big)_l^{n+1}\Delta t \\
&\qquad + \tfrac{\Delta t}{2i\sqrt{Re}}\Big(\big(\tfrac{\mathrm{D}}{\mathrm{DY}}\big)^4 - 2j^2\alpha^2\big(\tfrac{\mathrm{D}}{\mathrm{DY}}\big)^2 + j^4\alpha^4\Big)\Bigg]\hat{v}_{j,l}^{n+1} \\
&= \Bigg[\Big(\tfrac{i}{\sqrt{Re}} + \tfrac{1}{2}j\alpha\bar{u}_l^{n}\Delta t\Big)\Big(\big(\tfrac{\mathrm{D}}{\mathrm{DY}}\big)^2 - j^2\alpha^2\Big) - \tfrac{1}{2}j\alpha\big(\tfrac{\partial^2\bar{u}}{\partial Y^2}\big)_l^{n}\Delta t \\
&\qquad - \tfrac{\Delta t}{2i\sqrt{Re}}\Big(\big(\tfrac{\mathrm{D}}{\mathrm{DY}}\big)^4 - 2j^2\alpha^2\big(\tfrac{\mathrm{D}}{\mathrm{DY}}\big)^2 + j^4\alpha^4\Big)\Bigg]\hat{v}_{j,l}^{n} \\
&+ \tfrac{\Delta t}{2}\big(3\mathrm{N}\hat{v}_{j,l}^{n} - \mathrm{N}\hat{v}_{j,l}^{n-1}\big)
\end{aligned}
\tag{3.12}
$$

for $l = 2, 3, ..., N-2$, where

$$
\begin{aligned}
\mathrm{N}\hat{v}_{j,l}^{n} = i\sum_{\substack{k=-M\\k\neq 0,j}}^{M+j}&\Bigg[jk\alpha^2\Big(\frac{\mathrm{D}\hat{v}_{k,l}^{n}}{\mathrm{DY}}\hat{v}_{j-k,l}^{n} - \frac{k}{j-k}\hat{v}_{k,l}^{n}\frac{\mathrm{D}\hat{v}_{j-k,l}^{n}}{\mathrm{DY}}\Big) + \frac{j}{j-k}\frac{\mathrm{D}^2\hat{v}_{k,l}^{n}}{\mathrm{DY}^2}\frac{\mathrm{D}\hat{v}_{j-k,l}^{n}}{\mathrm{DY}} \\
&- \frac{j}{k}\frac{\mathrm{D}^3\hat{v}_{k,l}^{n}}{\mathrm{DY}^3}\hat{v}_{j-k,l}^{n}\Bigg] + j\alpha\Big(\hat{u}_0\frac{\mathrm{D}^2\hat{v}_{j,l}^{n}}{\mathrm{DY}^2} - j^2\alpha^2\hat{u}_0\hat{v}_{j,l}^{n} - \frac{\mathrm{D}^2\hat{u}_0}{\mathrm{DY}^2}\hat{v}_{j,l}^{n}\Big),
\end{aligned}
\tag{3.13}
$$

for $j = -M, -M+1, -M+2, ..., -1$, and

$$
\begin{aligned}
\mathrm{N}\hat{v}_{j,l}^{n} = i\sum_{\substack{k=-M+j\\k\neq 0,j}}^{M}&\Bigg[jk\alpha^2\Big(\frac{\mathrm{D}\hat{v}_{k,l}^{n}}{\mathrm{DY}}\hat{v}_{j-k,l}^{n} - \frac{k}{j-k}\hat{v}_{k,l}^{n}\frac{\mathrm{D}\hat{v}_{j-k,l}^{n}}{\mathrm{DY}}\Big) + \frac{j}{j-k}\frac{\mathrm{D}^2\hat{v}_{k,l}^{n}}{\mathrm{DY}^2}\frac{\mathrm{D}\hat{v}_{j-k,l}^{n}}{\mathrm{DY}} \\
&- \frac{j}{k}\frac{\mathrm{D}^3\hat{v}_{k,l}^{n}}{\mathrm{DY}^3}\hat{v}_{j-k,l}^{n}\Bigg] + j\alpha\Big(\hat{u}_0\frac{\mathrm{D}^2\hat{v}_{j,l}^{n}}{\mathrm{DY}^2} - j^2\alpha^2\hat{u}_0\hat{v}_{j,l}^{n} - \frac{\mathrm{D}^2\hat{u}_0}{\mathrm{DY}^2}\hat{v}_{j,l}^{n}\Big),
\end{aligned}
\tag{3.14}
$$

for $j = 1, 2, 3, ..., M$. In these expressions, the superscript represents the time level, the first subscript indicates the mode, and the second subscript refers to the grid.

Similarly, the discrete values of the mean flow correction are governed by

$$
\begin{aligned}
\Big(1 - \tfrac{\Delta t}{2}\big(\tfrac{\mathrm{D}}{\mathrm{DY}}\big)^2\Big)\hat{u}_{0,l}^{n+1} &= \Big(1 + \tfrac{\Delta t}{2}\big(\tfrac{\mathrm{D}}{\mathrm{DY}}\big)^2\Big)\hat{u}_{0,l}^{n} \\
&- \frac{i\sqrt{Re}\Delta t}{2\alpha}\sum_{\substack{k=-M\\k\neq 0}}^{M}\Big(\tfrac{3}{k}\hat{v}_{(-k,l)}^{n}\frac{\mathrm{D}^2\hat{v}_{k,l}^{n}}{\mathrm{DY}^2} - \tfrac{1}{k}\hat{v}_{(-k,l)}^{n-1}\frac{\mathrm{D}^2\hat{v}_{k,l}^{n-1}}{\mathrm{DY}^2}\Big).
\end{aligned}
\tag{3.15}
$$

The boundary conditions for each mode $j \in [-M, -M+1, ..., M]$ are given by the discrete forms of (2.22) for v_j^{n+1}

$$\begin{aligned} \hat{v}_{j,0}^{n+1} &= 0, & \left(\frac{\mathrm{D}\hat{v}_j^{n+1}}{\mathrm{D}Y}\right)_0 &= 0, \\ \left(\frac{\mathrm{D}\hat{v}_j^{n+1}}{\mathrm{D}Y}\right)_N + \alpha\hat{v}_{j,N}^{n+1} &= 0, & \left(\frac{\mathrm{D}^2\hat{v}_j^{n+1}}{\mathrm{D}Y^2}\right)_N - \alpha^2\hat{v}_{j,N}^{n+1} &= 0, \end{aligned} \tag{3.16}$$

and (2.24) for the mean flow correction:

$$\hat{u}_{0,0}^{n+1} = 0, \quad \left(\frac{\mathrm{D}\hat{u}_0^{n+1}}{\mathrm{D}Y}\right)_N = 0 \cdot \tag{3.17}$$

The above equations constitute a linear set of equations for the unknowns $\hat{v}_{j,l}^{n+1}$, $j = -M, -M+1, ..., M$, $l = 0, 1, 2, ..., N$, where, again, N is taken to be 80. We use this simulation only as a check. The period-fitting technique discussed in §2.4 allows for a drastic increase in time step. However, stability considerations will not allow full advantage of this increase to be taken when the nonlinear terms are treated explicitly. The majority of the results presented in the following *Results* section were obtained using period fitting and Crank-Nicolson differencing for the nonlinear terms, resulting in a fully nonlinear set of algebraic equations to be solved at each time step. In this case, (3.12) is replaced by the discrete analogue of (2.37)

$$\begin{aligned} &\Bigg[\left(\frac{i}{\sqrt{Re}} + \frac{\Delta t}{2}\left(\frac{\omega}{\sqrt{Re}} - j\alpha\bar{u}_l^{n+1}\right)\right)\left(\left(\frac{\mathrm{D}}{\mathrm{D}Y}\right)^2 - j^2\alpha^2\right) + \frac{1}{2}j\alpha\left(\frac{\partial^2\bar{u}}{\partial Y^2}\right)_l^{n+1}\Delta t \\ &\quad + \frac{\Delta t}{2i\sqrt{Re}}\left(\left(\frac{\mathrm{D}}{\mathrm{D}Y}\right)^4 - 2j^2\alpha^2\left(\frac{\mathrm{D}}{\mathrm{D}Y}\right)^2 + j^4\alpha^4\right)\Bigg](v')_{j,l}^{n+1} \\ &= \Bigg[\left(\frac{i}{\sqrt{Re}} - \frac{\Delta t}{2}\left(\frac{\omega}{\sqrt{Re}} - j\alpha\bar{u}_l^{n}\right)\right)\left(\left(\frac{\mathrm{D}}{\mathrm{D}Y}\right)^2 - j^2\alpha^2\right) - \frac{1}{2}j\alpha\left(\frac{\partial^2\bar{u}}{\partial Y^2}\right)_l^{n}\Delta t \\ &\quad - \frac{\Delta t}{2i\sqrt{Re}}\left(\left(\frac{\mathrm{D}}{\mathrm{D}Y}\right)^4 - 2j^2\alpha^2\left(\frac{\mathrm{D}}{\mathrm{D}Y}\right)^2 + j^4\alpha^4\right)\Bigg](v')_{j,l}^{n} \\ &+ \frac{\Delta t}{2}\left(\mathrm{N}(v')_l^n + \mathrm{N}(v')_l^n\right), \end{aligned} \tag{3.18}$$

and (3.15) is replaced by

$$\begin{aligned} \left(1 - \frac{\Delta t}{2}\left(\frac{\mathrm{D}}{\mathrm{D}Y}\right)^2\right)\hat{u}_{0,l}^{n+1} &= \left(1 + \frac{\Delta t}{2}\left(\frac{\mathrm{D}}{\mathrm{D}Y}\right)^2\right)\hat{u}_{0,l}^{n} \\ &- \frac{i\sqrt{Re}\Delta t}{2\alpha}\sum_{\substack{k=-M \\ k\neq 0}}^{M}\frac{1}{k}\left(\hat{v}_{(-k,l)}^{n}\frac{\mathrm{D}^2\hat{v}_{k,l}^{n}}{\mathrm{D}Y^2} + \hat{v}_{(-k,l)}^{n+1}\frac{\mathrm{D}^2\hat{v}_{k,l}^{n+1}}{\mathrm{D}Y^2}\right). \end{aligned} \tag{3.19}$$

To solve the nonlinear set, at each time step we begin by making a guess for the solution which is a cubic extrapolation using the previous 4 time steps. Using this guess, we compute the nonlinear terms on the right-hand sides of equations (3.18) and (3.19), and then solve the resulting linear systems for new values of $v_{j,l}^{n+1}$ which serve as the new guesses in the iteration. The process is repeated until convergence.

To utilise period-fitting, we employ the discrete analogue of equation (2.37). The algorithm for solving the resulting nonlinear algebraic set of equations at each time step is then identical to that described above.

§4 Results

In this section, we present results for both the linear and nonlinear simulations. We begin, however, by presenting the initial conditions obtained by Orr-Sommerfeld analysis, and by the 1st and 2nd order corrections.

4.1 Initial Conditions

The discrete version of the Orr-Sommerfeld equation (3.6) and corresponding boundary conditions (3.7) is solved by fixing values of α and $\sqrt{Re}$ and solving the eigenvalue problem for the frequency ω and eigenfunction v_0'. The value of ω is generally complex with a positive imaginary part representing growth with time and a negative imaginary part indicating temporal decay. For particular pairs of α and $\sqrt{Re}$ a purely real ω results. Figure (4.1) shows the neutral Orr-Sommerfeld curve for time $t_0 = 0.25$. The results are identical to those given in Otto (1994). We present this figure for later reference.

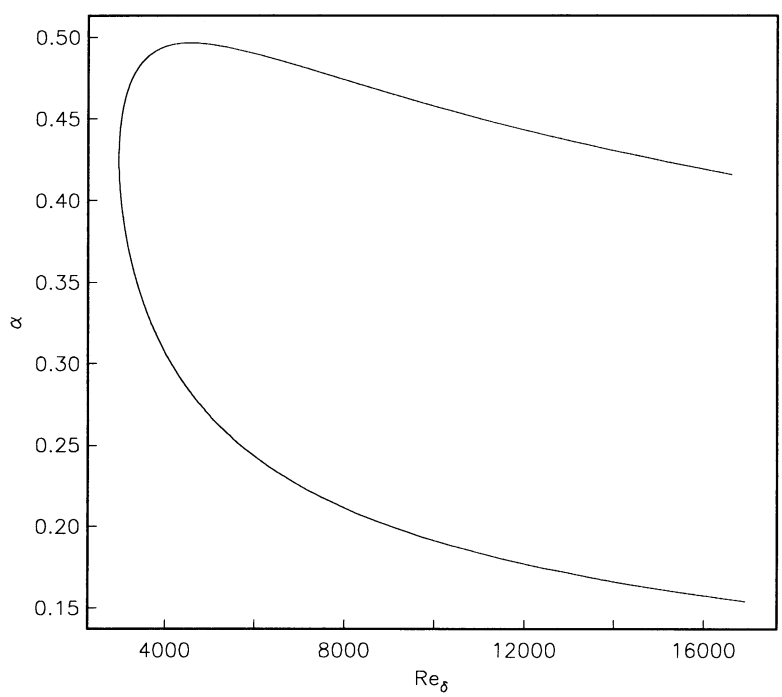

Figure 4.1 Neutral Orr–Sommerfeld curve showing the pairs of Reynolds number and streamwise wave number which give purely real ω

The reference values of α and $\sqrt{Re}$ we have chosen for our simulations are

$$\begin{aligned} \alpha &= 0.4 \\ \sqrt{Re} &= 3000 \end{aligned} \tag{4.1}$$

which defines a point just to the left of the neutral curve in figure (4.1). For these values, the corresponding ω resulting from the OS solution and the 1st and 2nd order corrections are given by

Orr-Sommerfeld:	$0.27589729 - 0.00004782i$
1st Order Correction	$0.27585418 + 0.00028591i$
2nd Order Correction	$0.27584836 + 0.00028872i$

and the resulting eigenfunctions, which may be used as initial conditions to the linear and nonlinear simulations, are presented in figures (4.2a) and (4.2b). Figure (4.2a) shows the real part of the initial profile, as generated by the OS analysis, which we call v_0^{OS}. In figure (4.2b), two curves are given. The dashed curve shows the deviation of the real part of the initial profile generated by the 1st order correction, v_0^1, from that generated by the OS analysis, v_0^{OS}. The dotted curve in this figure shows the deviation of the real part of the initial profile generated by the 2nd order correction, v_0^2, from that given by the 1st order correction. To plot both of these on the same graph, we scale the two curves appropriately, so the actual quantities seen on this figure are $|10^3 \frac{v_0^1 - v_0^{\mathrm{OS}}}{v_{0,\max}^{\mathrm{OS}}}|$ and $|10^4 \frac{v_0^2 - v_0^1}{v_{0,\max}^1}|$ vs. Y, where the denominators represent the peaks of these curves. This figure shows that the 1st order correction represents a 0.1% deviation from the OS curve, and the 2nd order correction deviates from the 1st order curve by about 0.005%. It will become evident in the linear simulations that the subtle differences between the initial conditions generated by each of these methods are important. It should also be noted that the OS equation predicts a stable mode while the corrected value represents an unstable one, for this pair of α and $\sqrt{Re}$.

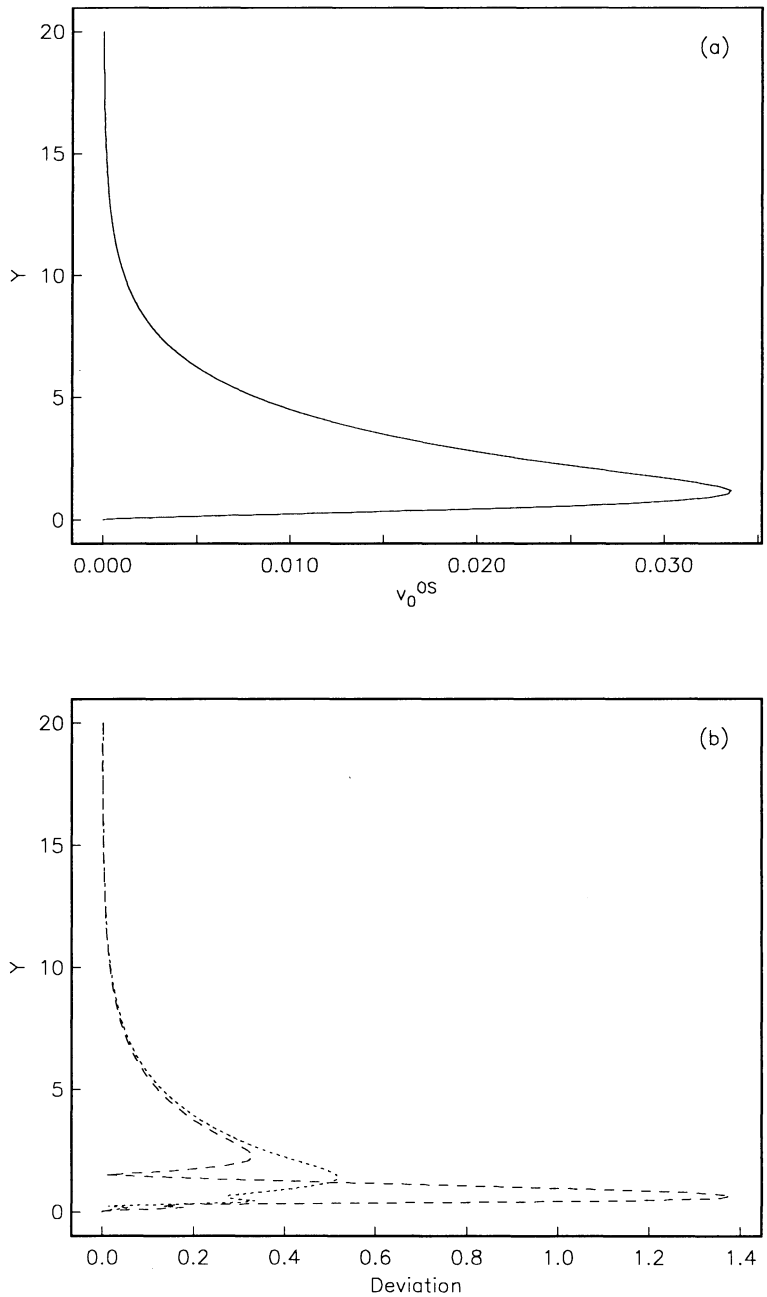

Figure 4.2 Initial Profiles for v. (a) Generated by OS analysis. (b) Scaled deviation between 1st order correction and OS (dashed), and between 2nd order correction and 1st order correction (dotted).

4.2 Linear Simulations

The linear simulations without period fitting are solutions to equations (3.10) at each time step. As results, we present the growth rate, $\mathrm{Im}(\omega)$, as a function of time, where ω is computed at each time step by equation (2.34). We note that a positive value of $\mathrm{Im}(\omega)$ indicates instability. We also point out that if $\bar{u}$ is fixed at its initial profile during the simulation, and not allowed to grow, this is equivalent to the parallel flow assumption and the value of ω should be constant in time and equal to the OS value. This provides an initial check of the simulation code, and is what we observed.

For the simulations without period fitting, the dispersive error in the Crank-Nicolson time differencing scheme makes the results very sensitive to the number of time steps used per period of oscillation. We begin by presenting results for a simulation which uses 200 time steps per initial period of oscillation; *i.e.*, Δt is chosen so that based upon the value of ω at $t = t_0$, one period of oscillation is divided into 200 grid points:

$$\Delta t = \frac{2\pi}{200\mathrm{Real}(\omega_0)}. \tag{4.2}$$

For this case, we give numerical solutions using each of the three initial conditions detailed in §2.3. Figure (4.3a) gives the results for the initial condition generated by the OS analysis (solid line), and the 1st order correction. It is evident that the nonphysical oscillations in the OS case are a result of the poor starting condition. The 1st order correction, which is sensitive to the evolution of the mean flow, eliminates most of the oscillations. The simulation using the initial condition generated by the 2nd order correction is free of oscillations on the graphical scale. This result is given in figure (4.3b).

Figure (4.4) gives the solutions corresponding to 100 (solid) and 50 (dashed) time steps per initial period of oscillation, respectively. The dotted curve on this figure is the 200 time step per period result given in figure (4.3b). We see that using 100 time steps per period is still ample, but that the quality of the results when 50 are used is markedly diminished due to dispersive error in the time-differencing scheme.

In figure (4.5), we give the results for the linear simulations with period fitting, using a time step equivalent to 10 (solid) and 2 (dashed) grid points per period, respectively. These are solutions to equations (3.11) at each time step. Again, the dotted curve on this figure is the 200 time step per period result of figure (4.3b). We note that we get results identical to this control case, using as few as 2 time steps per period.

We present two final figures associated with the linear simulations. Figure (4.6) shows Real(ω) versus time for the simulation with period fitting using 2 time steps per period, and demonstrates the effect of the mean flow evolution on the period of oscillation. In figure (4.7) we give a direct comparison between the growth rate predicted by OS theory at each time (dashed), versus the computed growth rate from the linear simulation (solid), again using the 2 time steps per period case. We see that the evolution has a significant destabilizing effect.

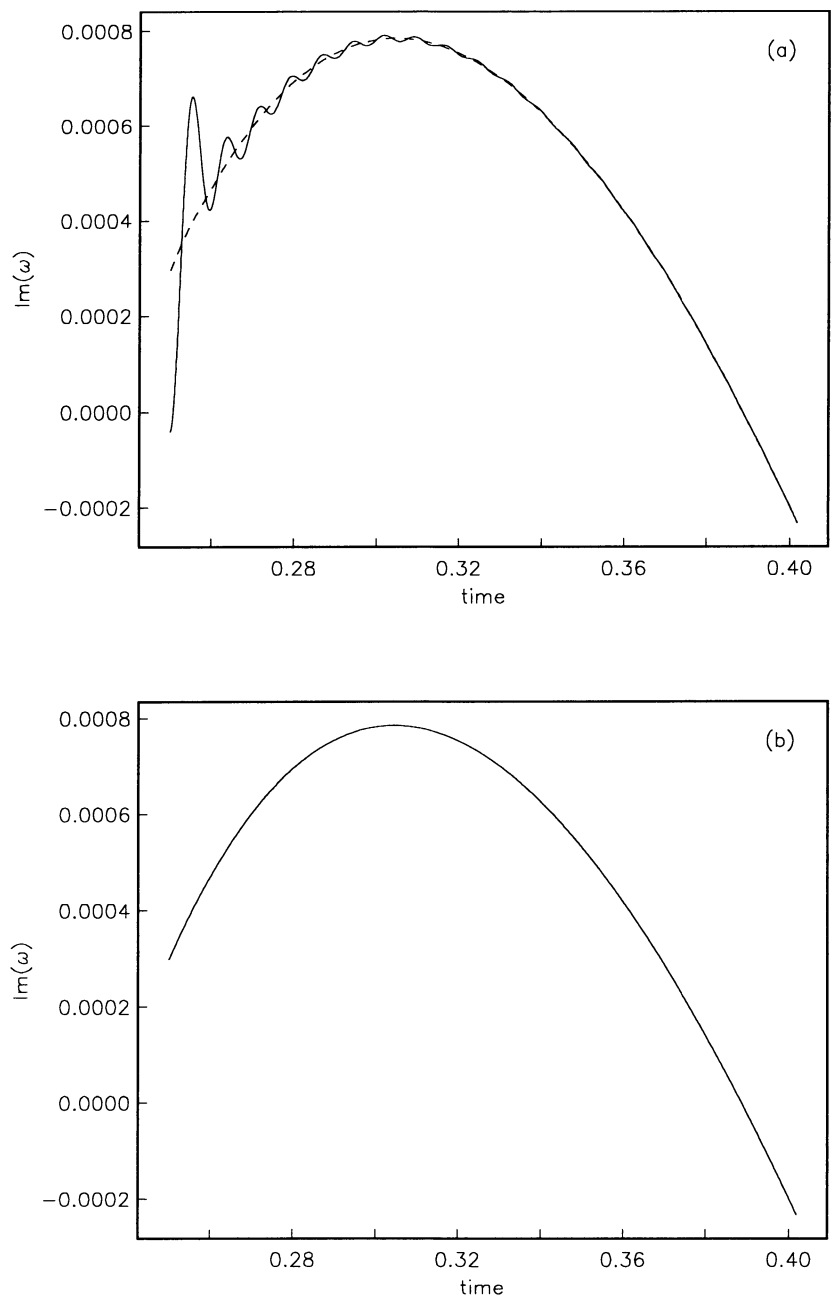

Figure 4.3 Linear Simulation. Duration: 20 periods, 200 time steps per period. Growth rate as a function of time. (a) OS (solid) and first order correction (dashed). (b) second order correction.

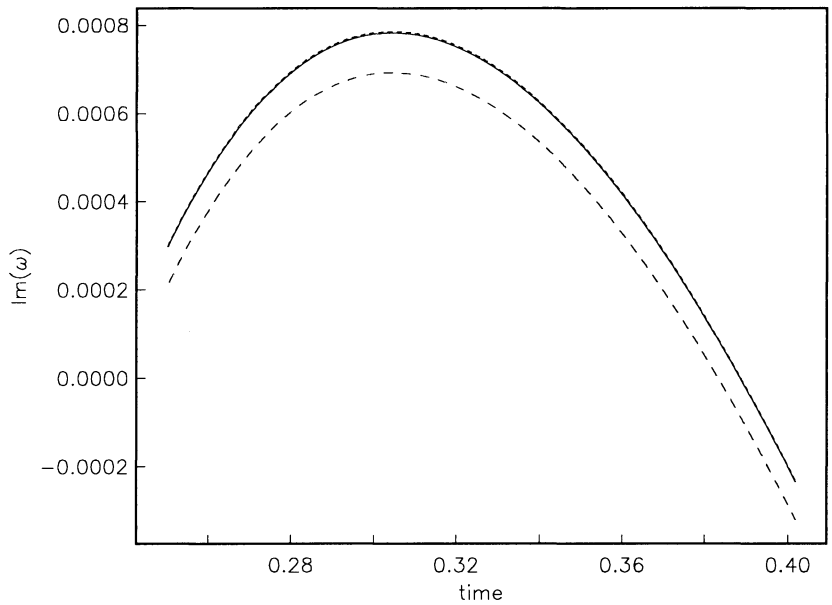

Figure 4.4 Linear Simulation without period fitting. Duration: 20 periods. Growth rate as a function of time. 100 (solid), 50 (dashed), and 200 (dotted) time steps per period.

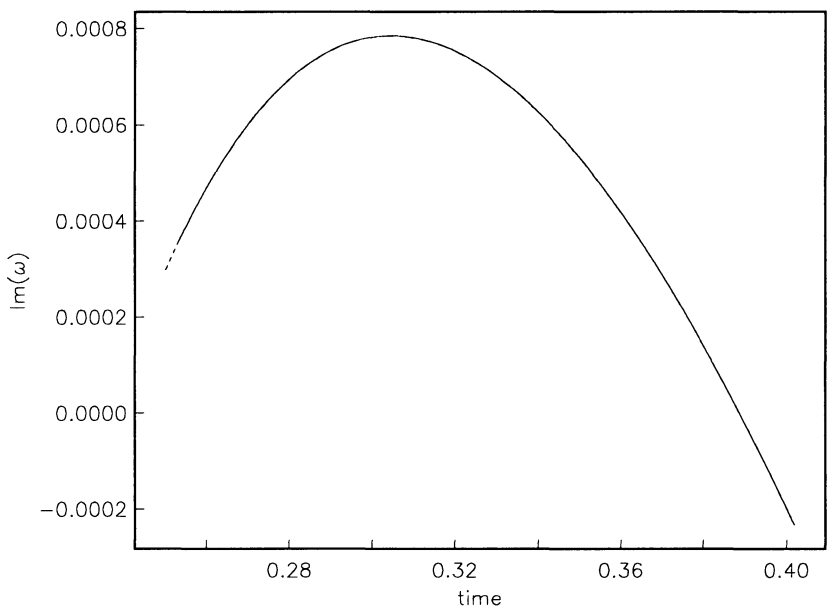

Figure 4.5 Linear Simulation with period fitting. Duration: 20 periods. Growth rate as a function of time. 10 (solid), 2 (dashed) and 200 (dotted) time steps per period.

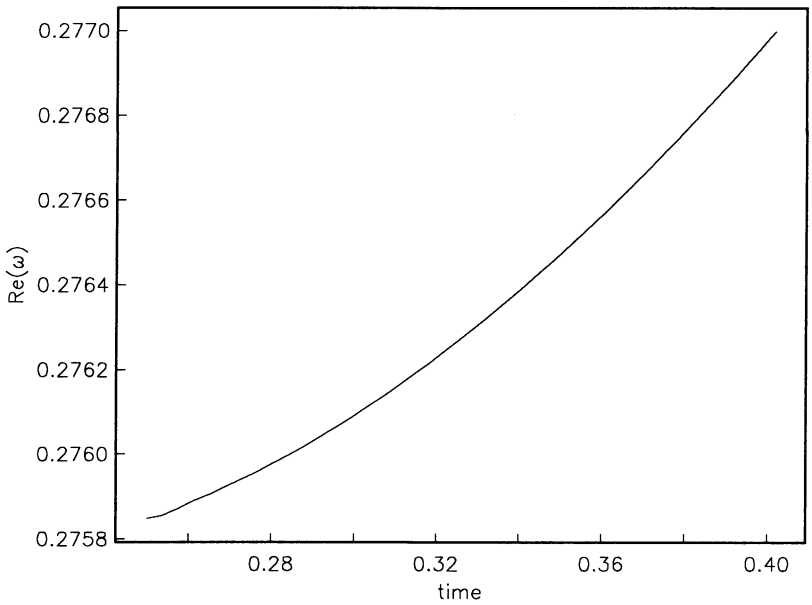

Figure 4.6 Linear Simulation with period fitting. Duration: 20 periods. 2 time steps per period. Period of oscillation as a function of time.

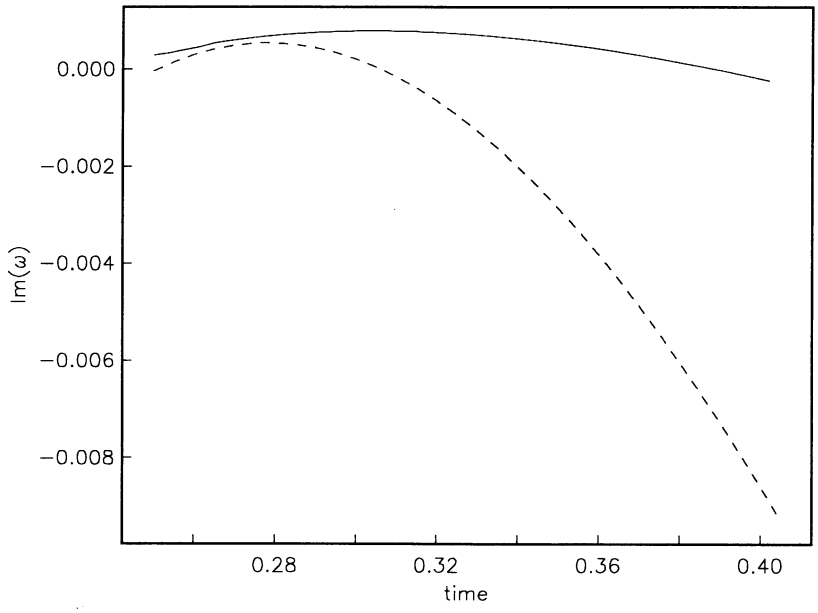

Figure 4.7 Comparison of Orr–Sommerfeld growth rate computed locally at each time step (dashed) versus growth rate computed from linear simulation which allows growth of the boundary layer (solid).

4.3 Nonlinear Simulations

For all the nonlinear simulations, we use the initial condition generated by the 2nd order correction for the $j = 1$ mode, and its conjugate for the $j = -1$ mode. However, we adjust the amplitude to test for the presence of nonlinear effects. All higher order modes are initially taken to have 0 values, as is the mean flow correction $\hat{u}_0$.

For the first four sets of simulation results, we used 17 modes ($j = -8, -7, ..., 8$) and we fixed the peak amplitude of the initial profile for the fundamental mode, given in figure (4.2), to be 0.000001 (figure 4.8), 0.002 (figure 4.9), 0.005 (figure 4.10) and 0.008 (figure 4.11). We employed the period fitting algorithm and used 40 time steps per one period of the fundamental mode. At each time step, the set of nonlinear equations given by (3.18) and (3.19), with boundary conditions (3.16) and (3.17) are solved. Each of these figures contains two graphs: the (a) part gives the growth rate of the fundamental mode, and in the (b) part, we present the energy curves for modes $j = 1$ to $j = 8$ where we define *energy* as $\ln(|\sqrt{E_j}|)$, and E_j is defined for the jth mode by equation (2.34). The strong oscillations exhibited in the higher order modes in figures (4.10) and (4.11) result from strongly nonlinear behaviour in the initial stages of the simulation, since all higher order modes are initially set to 0. This effect is amplified by aliasing errors.

On each of these figures, the dotted curve represents the results from the linear simulation which uses the same initial conditions. For the 0.000001 case, the linear results are obtained over the entire time range (dotted curve sits on the solution for the fundamental mode). However, even when the amplitude is as small as 0.002, the nonlinear effects can be seen within just a few periods.

To test the effects of even higher order terms, we repeat the 0.008 case above, using 33 modes ($j = -16, -15, ..., 16$). Again we use 40 time steps per one period of the fundamental mode. These results are presented in figure (4.12). In the (b) part of this figure, we again show only the modes $j = 1$ through $j = 8$. A reduction in oscillations occurs due to the elimination of aliasing errors; however, the startup effects can still be seen.

Finally, to verify that the period-fitting algorithm and nonlinear algebraic solver are working successfully for these simulations, we include a simulation where explicit 2nd order Adams-Bashforth temporal discretization is used to treat the nonlinear terms, and period fitting is not used. At each time step, we solve the linear set of equations (3.12) through (3.17). In this case, 400 time steps per one period of the fundamental period are used, and we include 16 modes. Figure (4.13) compares the growth rate of this simulation (20 periods in duration) with the first 20 periods of figure (4.11). It is evident that these algorithms are performing effectively.

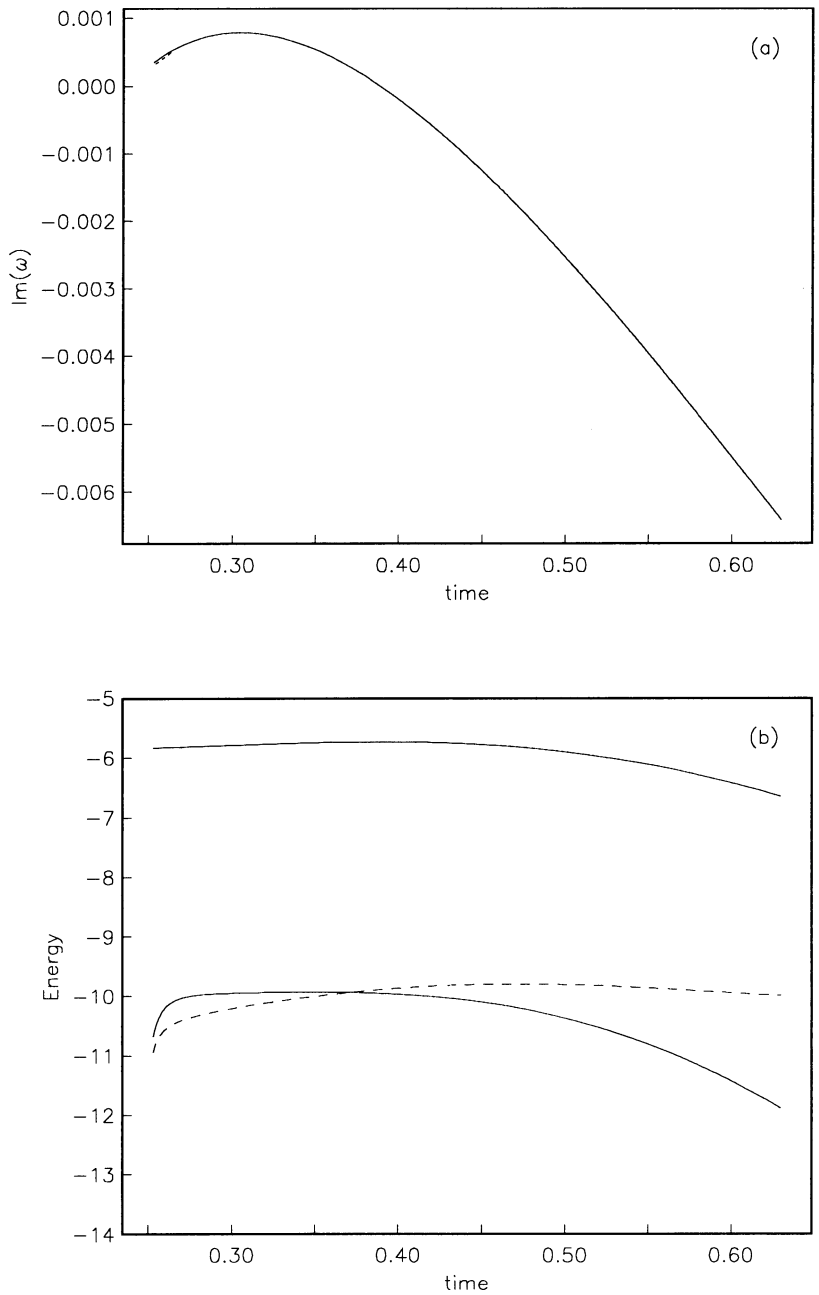

Figure 4.8 Nonlinear Simulation with period fitting. Duration: 50 periods. 17 modes. Initial amplitude of fundamental mode: 0.000001. (a) Growth rate of the fundamental mode. (b) Energy curves. Solid curves in (b) correspond to the first and second harmonics; dashed curve is the mean flow correction. Dotted curve in both figures is the linear result.

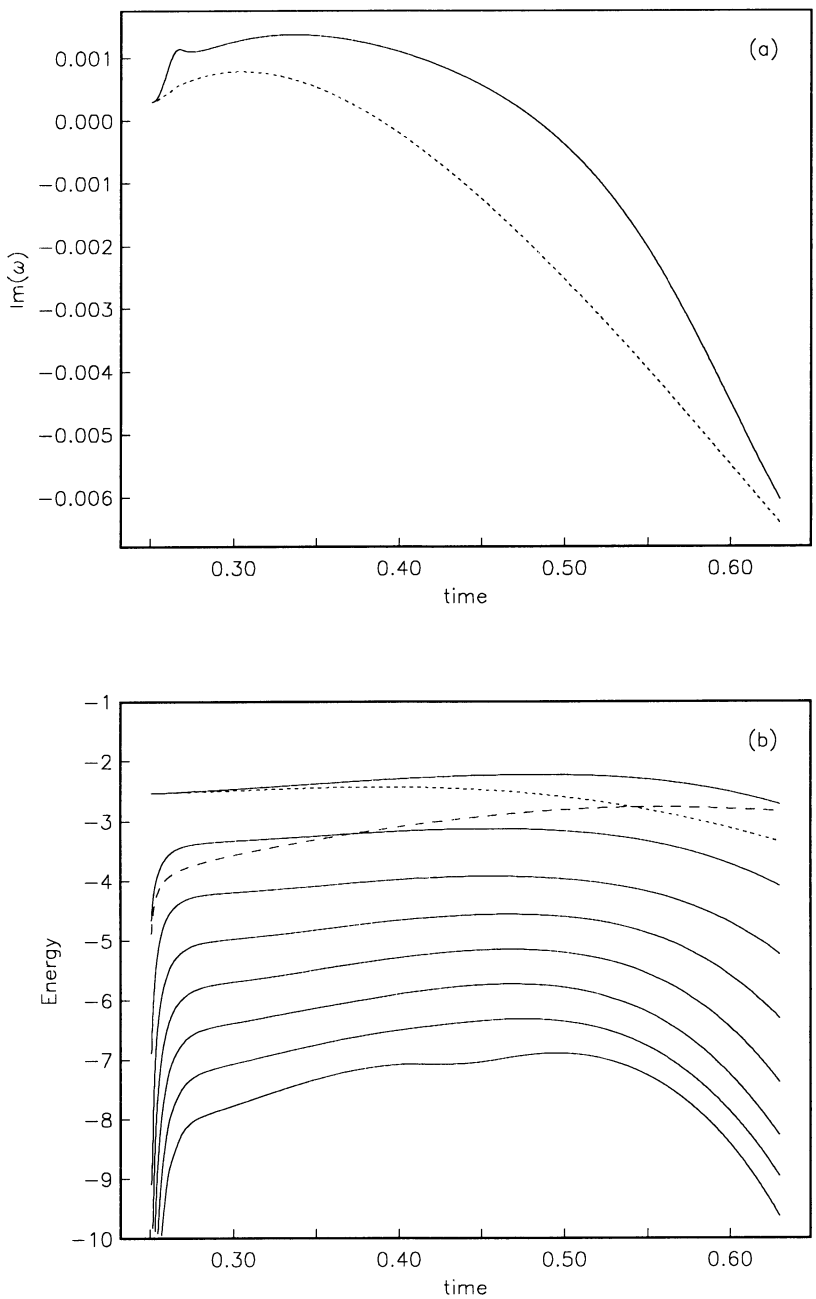

Figure 4.9 Nonlinear Simulation with period fitting. Duration: 50 periods. 17 modes. Initial amplitude of fundamental mode: 0.002. (a) Growth rate of the fundamental mode. (b) Energy curves. Dashed curve in (b) is the mean flow correction. Dotted curve in both figures is the linear result.

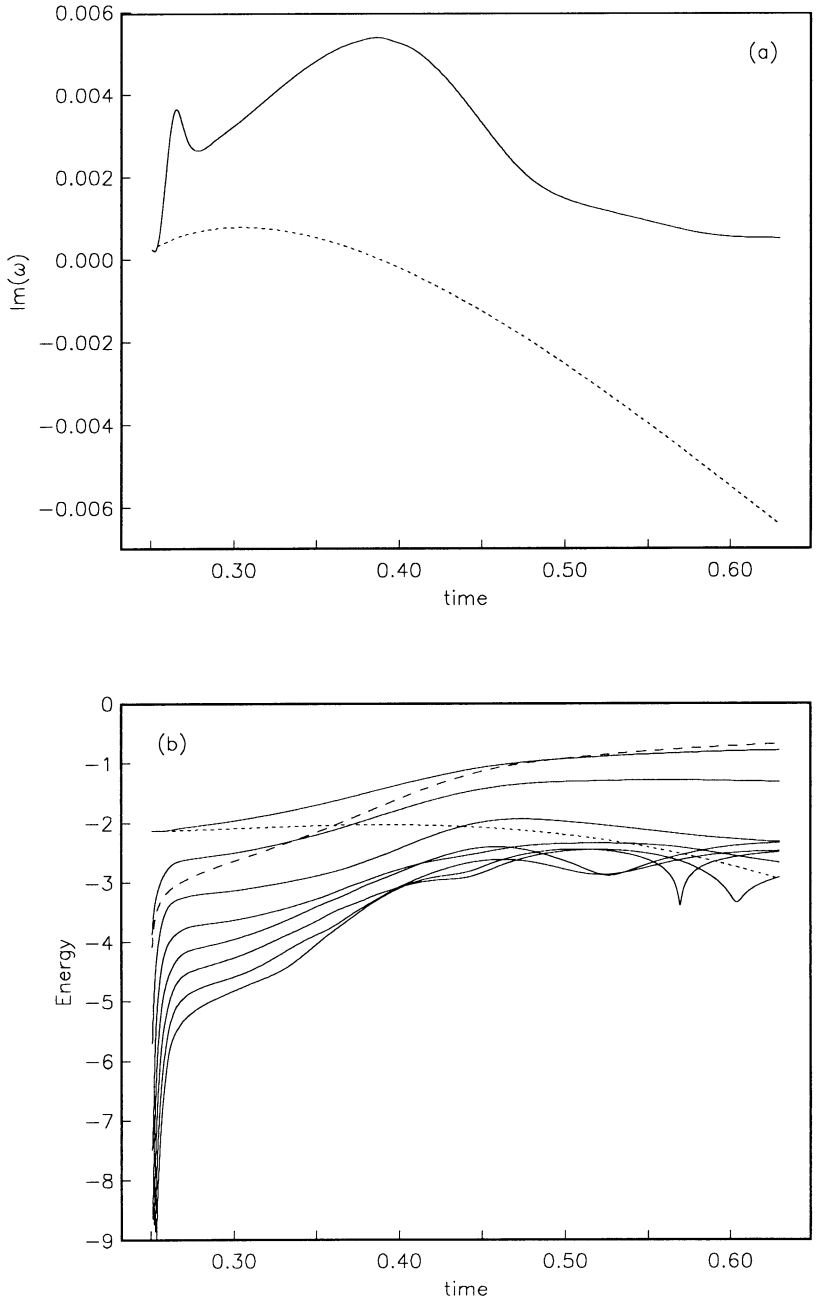

Figure 4.10 Nonlinear Simulation with period fitting. Duration: 50 periods. 17 modes. Initial amplitude of fundamental mode: 0.005. (a) Growth rate of the fundamental mode. (b) Energy curves. Dashed curve in (b) is the mean flow correction. Dotted curve in both figures is the linear result.

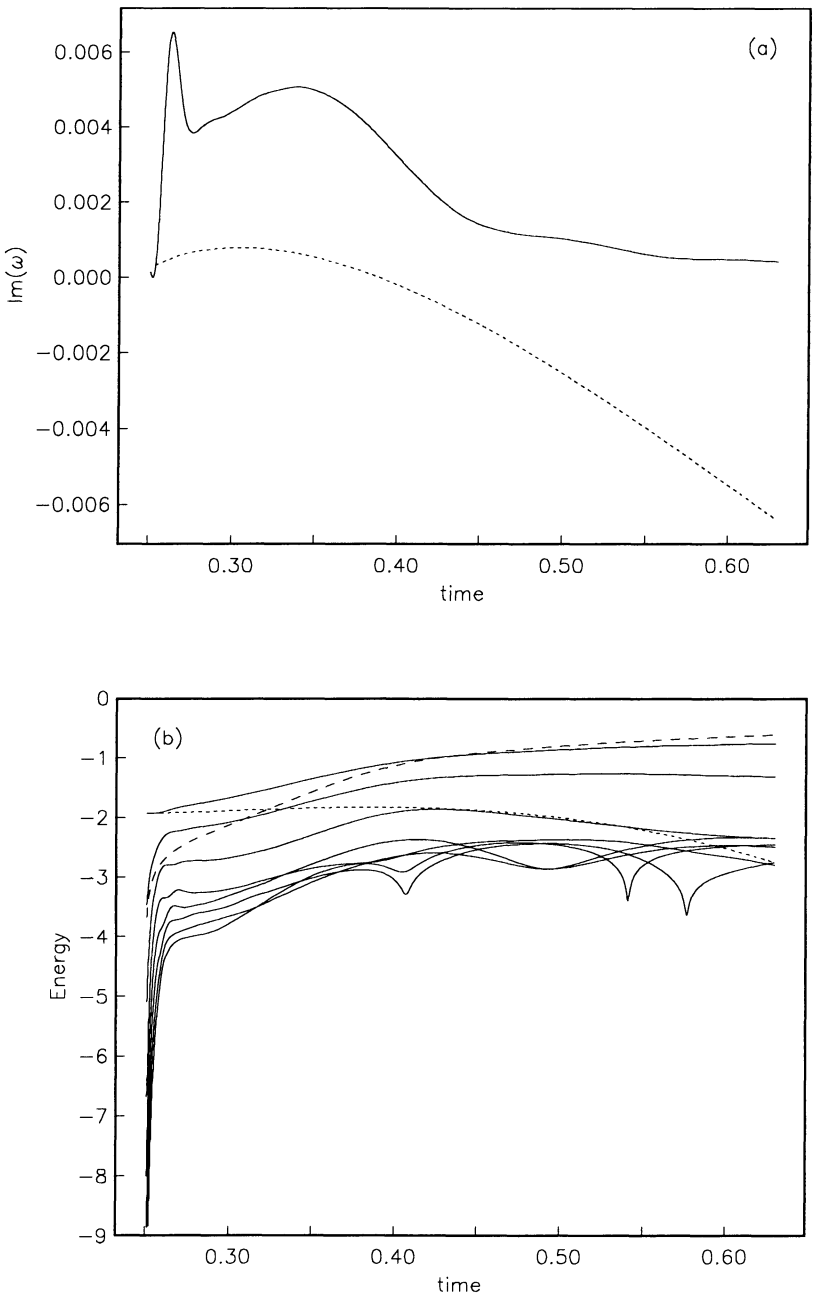

Figure 4.11 Nonlinear Simulation with period fitting. Duration: 50 periods. 17 modes. Initial amplitude of fundamental mode: 0.008. (a) Growth rate of the fundamental mode. (b) Energy curves. Dashed curve in (b) is the mean flow correction. Dotted curve in both figures is the linear result.

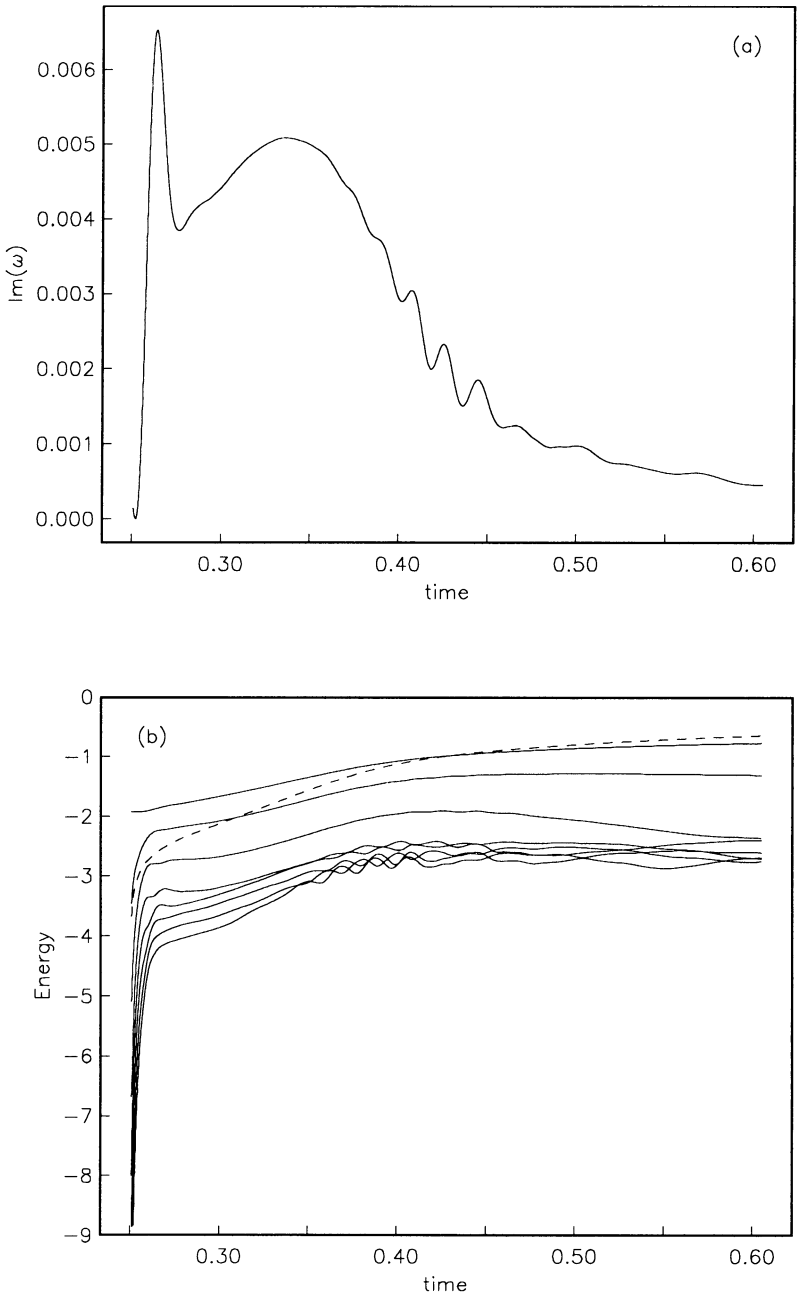

Figure 4.12 Nonlinear Simulation with period fitting. Duration: 50 periods. 33 modes. Initial amplitude of fundamental mode: 0.008. (a) Growth rate of the fundamental mode. (b) Energy curves. Dashed curve in (b) is the mean flow correction.

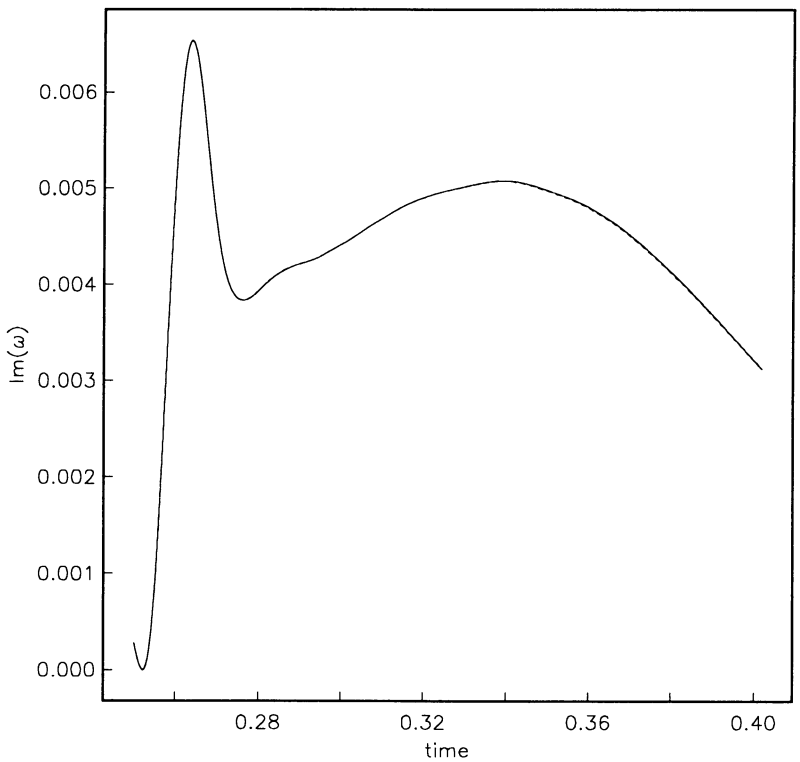

Figure 4.13 Nonlinear Simulation without period fitting. Explicit treatment of nonlinear terms. Duration: 20 periods. 17 modes. Initial amplitude of fundamental mode: 0.008. Growth rate of the fundamental mode is shown. Dotted curve is simulation associated with figure (4.11) – obscured.

§5 Conclusions

In this article we have endeavoured to describe how Tollmien–Schlichting waves may develop in a temporally evolving flow. We have shown, as is to be expected, that above a certain critical amplitude their presence will lead the situation to undergo some kind of transition. We have not tried to describe the flow within this régime, we have purely tried to demonstrate a possible mechanism which may lead to this state of affairs.

The main theme of our article is to develop reliable numerical techniques which allow us to solve the nonlinear partial differential equations that can arise in this kind of problem. The methods that have been used have been drawn from the evolution of so–called parabolising numerical techniques, both for instability work (see Bertolotti (1991)) and for full Navier–Stokes simulations (El-Hady (1989)). In our work we have the distinct advantage that our underlying physical problem evolves with time rather than a downstream coordinate, which renders the governing equations parabolic rather than elliptic as in the spatially evolving boundary layer case. This means that it is not necessary to change the characteristics of the equations to effect a cheap numerical solution, rather the methods can be exploited to provide more accurate solutions whilst using far less resolution, for instance by period fitting. In the PSE work, the spatially evolving wavenumber is taken to vary linearly with the downstream coordinate, so that the governing equations are no longer elliptic. If the next order terms were retained, the equations would revert to their previous state, whereas in our problem we are free to retain as high order variations as we choose. The assumption we choose to make is that we can fit a periodicity and the remainder of the evolution is on a slow scale.

In deriving initial conditions for our calculations we start with the Orr-Sommerfeld results, obtained by Otto (1994). As mentioned earlier we are aware that these results are fatally flawed, since they do not allow for the evolution of the undisturbed flow, but nevertheless they provide an initial guess for the modes' form and frequency. We then consider an eigenproblem in which we not only solve for the mode and complex

frequency, but also the temporal derivative of both quantities. In the example considered, this produces a fairly large change (rendering a mode that Orr-Sommerfeld predicts as stable to be unstable). This can be extended so that we ensure the second derivatives of the quantities are correct, producing minor modifications to the modes characteristics and eliminating just about all the visible transients from the growth rate curves (Figure 4.3). Unfortunately one problem that we have not resolved is the transients due to the start of the nonlinear modes; at the present we start our modes with zero amplitude (for the non–fundamental). We believe that this is what may be leading to the oscillations in the energy curves in figures (4.10b), (4.11b) and (4.12b).

Our simulations for the linear problem seem to produce the expected results; that is, the flow can support Tollmien–Schlichting waves for a finite time interval. In the simulation associated with figure (4.7), it appears that the evolution of the mean flow has a significant destabilising effect, but it should be noted that the OS analysis, to which we are making comparisons, is suspect when applied to this evolutionary flow situation: in Section 4.1, we point out that the OS analysis predicts a stable mode where the corrected cases suggest instability (we appreciate that this mode is close to the neutral boundary). It should also be noted that even changing the quantity which represents the energy of the mode can significantly alter the results, as seen in Smith (1979a). Perhaps the main message to be taken from this part of the study is that one should consider the corrected Orr-Sommerfeld equation rather than the parallel one as the extra work is more than rewarded by the enhanced accuracy.

The nonlinear simulations are as would be expected, in that above a certain initial amplitude of the fundamental, after a period of growth, the modes will induce a transition. The development of this set of methods has enabled us to study these modes, and we are currently attempting to take this calculation further, perhaps on into the turbulent régime. It is likely that our modal calculations will have more success than the spatial calculations since our equations are actually truly parabolic.

We hope to extend this work into the compressible domain, so that a study of the unstable characteristics in the case of subsonic, transonic and supersonic plate speeds may be performed, and the noise radiation at high speeds predicted.

Acknowledgements

The authors would like to thank Drs. Craig L. Streett and M.Y. Hussaini for their invaluable insight throughout this work.

References

Bertolotti, F. P. (1991) Linear and Nonlinear Stability of Boundary Layers with Streamwise Varying Properties. *PhD Thesis, The Ohio State University*

Eagles, P. M. & Weismann, M. A. (1975) On the stability of slowly varying flow: the divergent channel *J. Fluid Mech.* **69** 241

El-Hady, N. M. (1991) Nonparallel Instability of Supersonic and Hypersonic Boundary Layers *AIAA-91-0324*

Gaster, M. (1974) On the Effects of Boundary Layer Growth on Flow Stability *J. Fluid Mech.* **66** 465

Hall P. & Smith, F. T. (1984) On the Effects of Nonparallelism, Three Dimensionality and Mode Interaction in Nonlinear Boundary-Layer Stability *Stud. Appl. Math.* **70** 91

Otto, S. R. (1994) On the stability of a Time Dependent Boundary Layer *submitted to Theor. Comp. Fluid Dyn.*

Smith, F. T. (1979a) On the non-parallel flow stability of the Blasius boundary layer *Proc. Roy. Soc. Lond. A.* **366** 91

Smith, F. T. (1979b) Nonlinear stability of boundary layers for disturbances of various sizes *Proc. Roy Soc. Lond. A.* **368** 573

REPORT DOCUMENTATION PAGE

Form Approved
OMB No. 0704-0188

Public reporting burden for this collection of information is estimated to average 1 hour per response, including the time for reviewing instructions, searching existing data sources, gathering and maintaining the data needed, and completing and reviewing the collection of information. Send comments regarding this burden estimate or any other aspect of this collection of information, including suggestions for reducing this burden, to Washington Headquarters Services, Directorate for Information Operations and Reports, 1215 Jefferson Davis Highway, Suite 1204, Arlington, VA 22202-4302, and to the Office of Management and Budget, Paperwork Reduction Project (0704-0188), Washington, DC 20503.

1. AGENCY USE ONLY *(Leave blank)*

2. REPORT DATE
May 1994

3. REPORT TYPE AND DATES COVERED
Contractor Report

4. TITLE AND SUBTITLE
ON THE NONLINEAR STABILITY
OF VISCOUS MODES WITHIN THE RAYLEIGH PROBLEM
ON AN INFINITE FLAT PLATE

5. FUNDING NUMBERS
C NAS1-19480
WU 505-90-52-01

6. AUTHOR(S)
J.C. Webb
S.R. Otto
G.M. Lilley

7. PERFORMING ORGANIZATION NAME(S) AND ADDRESS(ES)
Institute for Computer Applications in Science
and Engineering
Mail Stop 132C, NASA Langley Research Center
Hampton, VA 23681-0001

8. PERFORMING ORGANIZATION REPORT NUMBER
ICASE Report No. 94-30

9. SPONSORING/MONITORING AGENCY NAME(S) AND ADDRESS(ES)
National Aeronautics and Space Administration
Langley Research Center
Hampton, VA 23681-0001

10. SPONSORING/MONITORING AGENCY REPORT NUMBER
NASA CR-194909
ICASE Report No. 94-30

11. SUPPLEMENTARY NOTES
Langley Technical Monitor: Michael F. Card
Final Report
Submitted to the Journal of Fluid Mechanics

12a. DISTRIBUTION/AVAILABILITY STATEMENT
Unclassified–Unlimited
Subject Category 34

12b. DISTRIBUTION CODE

13. ABSTRACT *(Maximum 200 words)*

The stability has been investigated of the unsteady flow past an infinite flat plate when it is moved impulsively from rest, in its own plane. For small times the instantaneous stability of the flow depends on the linearised equations of motion which reduce in this problem to the Orr-Sommerfeld equation. It is known that the flow for certain values of Reynolds number, frequency and wavenumber is unstable to Tollmien-Schlichting waves, as in the case of the Blasius boundary layer flow past a flat plate. With increase in time, the unstable waves only undergo growth for a finite time interval, and this growth rate is itself a function of time. The influence of finite amplitude effects is studied by solving the full Navier-Stokes equations. It is found that the stability characteristics are markedly changed both by the consideration of the time evolution of the flow, and by the introduction of finite amplitude effects.

14. SUBJECT TERMS
Rayleigh layer, nonlinear, stability

15. NUMBER OF PAGES
41

16. PRICE CODE
A03

17. SECURITY CLASSIFICATION OF REPORT
Unclassified

18. SECURITY CLASSIFICATION OF THIS PAGE
Unclassified

19. SECURITY CLASSIFICATION OF ABSTRACT

20. LIMITATION OF ABSTRACT